analytical chemistry

Article

Cite This: Anal. Chem. 2018, 90, 8116–8122

pubs.acs.org/ac

Simultaneous Detection of Mitochondrial Hydrogen Selenide and Superoxide Anion in HepG2 Cells under Hypoxic Conditions

Ranran Cheng,‡ Fanpeng Kong,‡ Lili Tong, Xiaojun Liu, Kehua Xu,* and Bo Tang*

College of Chemistry, Chemical Engineering and Materials Science, Institute of Biomedical Sciences, Collaborative Innovation Center of Functionalized Probes for Chemical Imaging in Universities of Shandong, Key Laboratory of Molecular and Nano Probes, Ministry of Education, Shandong Provincial Key Laboratory of Clean Production of Fine Chemicals, Shandong Normal University, Jinan 250014, People's Republic of China

Supporting Information

ABSTRACT: Previous studies proposed that sodium selenite (Na_2SeO_3) was reduced to hydrogen selenide (H_2Se) and that H_2Se subsequently reacted with oxygen to generate superoxide anion ($O_2^{\bullet-}$), resulting in tumor cell oxidative stress and apoptosis. However, under the hypoxic conditions of a solid tumor, the anticancer mechanism of sodium selenite remains unclear. To reveal the exact anticancer mechanism of selenite in the real tumor microenvironment, we developed a mitochondria-targeting fluorescent nanosensor, Mito-N-D-MSN, which was fabricated from mesoporous silica nanoparticles (MSNs) loaded with two small-molecule fluorescent probes and a triphenylphosphonium ion as a mitochondria-targeting moiety. With Mito-N-D-MSN, the fluctuations in the contents of mitochondrial hydrogen selenide (H_2Se) and superoxide anion ($O_2^{\bullet-}$) in HepG2 cells induced by Na_2SeO_3 were investigated in detail under normoxic and hypoxic conditions. The results showed that the mitochondrial H_2Se content increased gradually, while the $O_2^{\bullet-}$ content remained unchanged in HepG2 cells under hypoxic conditions, which indicated that the anticancer mechanism of selenite involves nonoxidative stress in the real tumor microenvironment.

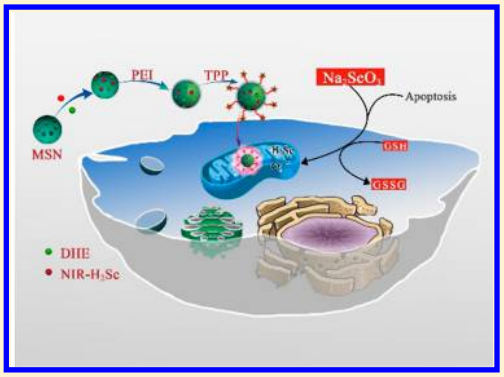

Selenium is an important micronutrient with essential biological functions[1] and has cancer chemopreventive properties.[2,3] Recently, research on the protective effects of selenium against cancer has received increasing attention,[4−6] but the detailed molecular mechanisms by which selenium kills cancer cells remain elusive. It is considered that the anticancer mechanism of selenium is closely associated with oxidative stress (as shown in Scheme 1), in which selenite is reduced to hydrogen selenide (H_2Se),[7,8] and H_2Se subsequently reacts with oxygen to generate and accumulate superoxide anion ($O_2^{\bullet-}$), resulting in tumor cell oxidative stress and apoptosis.[9,10] However, previous studies at the cellular level involved culturing with Na_2SeO_3 in a normal oxygen environment and did not take into account the hypoxic environment of solid tumors. To precisely determine the anticancer mechanism of selenite, it is urgent to research the changes in H_2Se and $O_2^{\bullet-}$ levels simultaneously in hypoxic environments.

Scheme 1. Potential Mechanism of Sodium Selenite Anticancer Effect

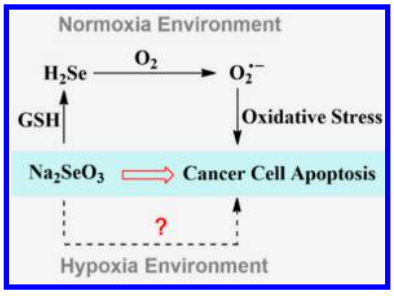

Fluorescence probes have been recognized as one of the most efficient molecular tools for biological systems due to their high sensitivity and selectivity, real-time imaging ability, and nondestructive detection.[11−13] A number of small-molecule fluorescent probes for the selective detection of H_2Se and $O_2^{\bullet-}$ have been developed sequentially.[14−16] However, the simultaneous detection of H_2Se and $O_2^{\bullet-}$ has not been reported thus far. Moreover, it is difficult to accurately detect H_2Se and $O_2^{\bullet-}$ at the same position in cells using two different small-molecule fluorescent probes.

To simultaneously achieve the real-time monitoring of mitochondrial H_2Se and $O_2^{\bullet-}$ changes, we developed a mitochondria-targeting fluorescent nanoprobe Mito-N-D-MSN to simultaneously monitor the changes in H_2Se and $O_2^{\bullet-}$ in HepG2 cells induced by Na_2SeO_3 under hypoxic conditions for the first time (Scheme 2). Mito-N-D-MSN was composed of four units: (1) mesoporous silica nanoparticles

Received: March 25, 2018
Accepted: June 8, 2018
Published: June 8, 2018

DOI: 10.1021/acs.analchem.8b01345
Anal. Chem. 2018, 90, 8116–8122

Scheme 2. Schematic Illustration of Mito-N-D-MSN Monitoring the Mitochondrial H_2Se and $O_2^{\bullet-}$ Concentrations Level in HepG2 Cells Induced by Na_2SeO_3

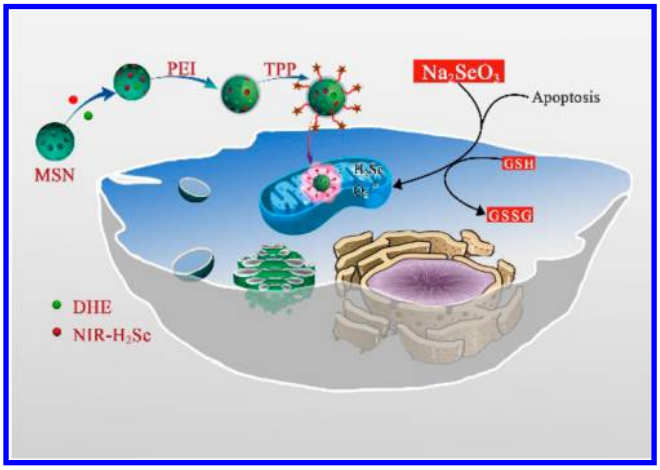

(MSNs), which had good biocompatibility, a high loading capacity, and easy functionalization;[17−19] (2) a molecular fluorescence probe, NIR-H_2Se for H_2Se and DHE for $O_2^{\bullet-}$ (the emission wavelengths of DHE[20,21] and NIR-H_2Se[22] were 638 and 735 nm, respectively, which could be resolved effectively (Figure S1); (3) polyethylenimine (PEI), which was attached to the surface of the MSNs via electrostatic interactions to block the pores; and (4) triphenylphosphonium (TPP) ion as a mitochondria-targeting moiety. By utilizing Mito-N-D-MSN, the changes in mitochondrial H_2Se and $O_2^{\bullet-}$ concentration levels in HepG2 cells induced by Na_2SeO_3 under normoxic conditions and hypoxic conditions were sufficiently studied. The results showed that under hypoxic conditions and after induction by Na_2SeO_3, the mitochondrial H_2Se in HepG2 cells was present at a high level and accumulated gradually, while the mitochondrial $O_2^{\bullet-}$ contents were low and remained unchanged. This study indicated that the anticancer mechanism of selenite is connected to nonoxidative stress under hypoxic conditions.

EXPERIMENTAL SECTION

Materials and Instruments. All chemicals and solvents were used as received unless otherwise stated. Ultrapure water was obtained from a Millipore water ultrapurification system. Transmission electron microscopy (TEM) was performed on a JEM-100CX-II electron microscope. UV−vis absorption analysis was carried out on a UV-1700-vis spectrometer (Shimadzu, Japan). The pH was measured using a pH-3 digital pH meter. Fluorescence spectra were recorded on an Edinburgh FLS-920 fluorescence spectrophotometer.

Preparation of Mesoporous Silica Nanoparticles. The 40 nm MSNs were synthesized according to a reported protocol with some modifications.[23−25] Hexadecyltrimethylammonium bromide (CTAB, 0.7657 g) was added to 50 mL of distilled water, and 154.2 μL of trolamine (TEA) was added. Then, the mixture was heated to 80 °C under intense stirring for 30 min. Subsequently, 7 mL of tetraethyl orthosilicate (TEOS) was added dropwise with stirring for another 1 h. To remove the residual reactants, the products were washed with methanol and ethanol several times. Finally, to completely remove the CTAB remaining inside the mesopores, the collected products were calcined at 450 °C for 10 h.

Assembly of the Nanoprobe. Then, 0.1 mg/mL NIR-H_2Se and 0.05 mg/mL DHE were added to 1 mL of the as-prepared MSN (1 mg/mL) solution at room temperature in darkness with gentle stirring overnight. Excess NIR-H_2Se and DHE were removed after centrifugation and washing the nanoparticles with distilled water several times. Next, 0.2 mg/mL PEI was added with stirring at room temperature for another 24 h in darkness to activate amino groups, 0.5 mM TPP and 1.5 mM EDC solutions were added and reacted for 30 min at room temperature in darkness to activate carboxylate groups, and 2 mM NHS was added to form amido bonds.[26] The resulting precipitates were centrifuged (12000 rpm, 10 min) and washed three times with distilled water.

Quantitation of the NIR-H_2Se and DHE Loaded on the Nanoprobe. A total of 1 μL of nanoprobe (0.1 mg/mL) solution was heated at 70 °C in a water bath for 1 h. The nanoprobe solution was then centrifuged (12000 rpm, 10 min), and the precipitates were redispersed in 1 mL of PBS buffer (10.0 mM, pH 7.4); then, this process was repeated to completely release NIR-H_2Se and DHE from the pores. Subsequently, the fluorescence intensity of the supernate was measured. According to the standard linear calibration curves of NIR-H_2Se and DHE, the concentrations in the pores were determined.

Fluorescence Measurements. For the detection of H_2Se, H_2Se was prepared by the reaction of Al_2Se_3 with H_2O in an N_2 atmosphere for 30 min at room temperature before use. The fluorescence response of the nanoprobe toward different amounts of H_2Se was measured in pH 7.8 buffers, in which the mitochondria had a slightly basic pH of approximately 7.8.[27,28] Different concentrations of H_2Se were added to the nanoprobe solution (0.1 mg/mL) to detect the fluorescence response. The fluorescence spectra were collected with $\lambda_{ex}/\lambda_{em}$ = 688/735 nm.

For the detection of $O_2^{\bullet-}$, $O_2^{\bullet-}$ was prepared by dissolving KO_2 in DMSO solution. The concentration of $O_2^{\bullet-}$ was determined on the basis of the various concentrations of KO_2.[29] Various amounts of $O_2^{\bullet-}$ were added to the nanoprobe solution (0.1 mg/mL) to detect the fluorescence response. The fluorescence intensity was measured at $\lambda_{ex}/\lambda_{em}$ = 488/638 nm.

The effects of a pH from 4.0 to 9.0 on the fluorescence intensities of the nanoprobe in response to H_2Se and $O_2^{\bullet-}$ in PBS (10.0 mM) were investigated. Then, the selectivity of the nanoprobe for H_2Se and $O_2^{\bullet-}$ was evaluated by adding interferences, such as H^+, metal ions, oxidative-stress-associated redox chemicals, biologically relevant and ROSs.[30] To evaluate the selectivity of the nanoprobe for H_2Se and $O_2^{\bullet-}$, we tested H^+; metal ions (K^+, Ca^{2+}, Na^+, Mg^{2+}, Cu^{2+}, Fe^{2+}, Fe^{3+}, Ni^+, Zn^{2+}, Cd^{2+}); and the reactivity of NIR-H_2Se to biologically relevant ROSs including H_2O_2, $ROO^{\bullet}$, and ^-OCl and oxidative-stress-associated redox chemicals such as glutathione (GSH), cysteine (Cys), homocysteine (Hcy), Sec, H_2S, Na_2SeO_3, thioredoxin reductase (TrxR), *N*-acetyl-L-cysteine (NAC), and vitamin C (Vc).

The responses of the nanoprobe to H_2Se and $O_2^{\bullet-}$ were evaluated via a kinetics experiment to verify the fast response for H_2Se and $O_2^{\bullet-}$ detection. We first recorded a time course of the fluorescence intensity of a 0.1 mg/mL nanoprobe with 25 μM H_2Se in PBS buffer (10.0 mM, pH 7.8) for 15 min and then continued to add 25 μM H_2Se, recording the intensity for another 15 min. Then, the same kinetics experiment was performed for $O_2^{\bullet-}$.

DOI: 10.1021/acs.analchem.8b01345
Anal. Chem. 2018, 90, 8116−8122

TEM Assay. HepG2 cells were treated with 0.1 mg/mL nanoprobe for 4 h, fixed in fresh 2.5% glutaraldehyde for at least 4 h at 4 °C, postfixed in 1% osmium tetroxide for 1.5 h, dehydrated in a gradient ethanol series and infiltrated with Epon 812. The samples were then embedded and cured at 37 °C for 12 h, 45 °C for 12 h and 60 °C for 24 h. Ultrathin sections were cut and stained with uranyl acetate and lead citrate before observation. Then, the cells were trypsinized, centrifuged, fixed in 2.5% glutaraldehyde in 0.1 M sodium cacodylate buffer (pH 7.4) for 1 h at room temperature and rinsed. Cells were then postfixed for 1 h in 2% osmium tetroxide with 3% potassium ferrocyanide and rinsed, followed by en bloc staining with a 2% aqueous uranyl acetate solution, dehydration with a graded series of alcohol, two exchanges with propylene oxide, a series of propylene oxide/Epon dilutions, and embedding in 100% Epon. The thin (70 nm) sections were cut on a Leica UC6 ultramicrotome, and images were recorded on a JEOL 1200EX (JEOL, Ltd. Tokyo, Japan) using an AMT 2k digital camera.

Cell Culture. HepG2 cells were cultured in Dulbecco's modified Eagles medium (DMEM) with 100 U/mL of 1% penicillin/streptomycin and 10% fetal bovine serum. The cultures were maintained at 37 °C in a 100% humidified atmosphere containing 5% CO_2/95% air (20% O_2) and 95% CO_2/5% air (1% O_2) for normoxic and hypoxic conditions, respectively, in an incubator (MCO-15AC, Sanyo, Tokyo, Japan).

Cytotoxicity Assay. The cytotoxicity of the nanoprobe was evaluated by the standard MTT assay. HepG2 cells were cultured in 96-well microtiter plates and incubated in 5% CO_2 at 37 °C for 24 h. After the original medium was removed, the cells were incubated with the nanoprobe (0, 0.1, 0.2, 0.3 mg/mL) for 6, 12, and 24 h, respectively. Next, 150 μL of MTT solution (0.5 mg/mL) was added to each well. After 4 h, the remaining MTT solution was removed, and 150 μL of DMSO was added to each well to dissolve the formazan crystals. We used the RT 6000 microplate reader to measure the absorbance. The experiment was repeated three times, and the data are shown as the mean ± SD.

Colocalization Fluorescence Imaging. Considering that the variations in the H_2Se and $O_2^{\bullet-}$ contents in mitochondria are unclear, we assembled Mito-Cy5-MSN by loading Cy5, a bright NIR fluorescent dye, instead of DHE and NIR-H_2Se and modified the mitochondria-targeting moiety to improve the veracity in the colocalization experiments. The HepG2 cells were incubated with 0.1 mg/mL Mito-Cy5-MSN for 6 h, washed three times with PBS (pH 7.4), incubated with MitoTracker Green (MTG, 100 nM) for 10 min, and washed three times with PBS. The fluorescence images were recorded in two channels. The green channel had excitation at 488 nm and a collection window of 550−650 nm, and the red channel captured images using a 633 nm laser and an emission filter at 650−750 nm. For a better comparison, we incubated Calcein, AM, Ultrapure grade (CAUG, 50 nM) and LysoTracker DND-26 (LTD, 100 nM) with the same method above. The colocalization ratio of the nanoprobe was quantified by Image-Pro Plus imaging software. Pearson's correlation coefficient was measured with more than 50 cells and calculated from the mean data of the cells.

Confocal Fluorescence Imaging. Considering that the real solid tumor microenvironment is hypoxia because of leaky and dysfunctional tumor vasculature,[31] the detection of the changes in H_2Se and $O_2^{\bullet-}$ in the mitochondria of HepG2 cells induced by Na_2SeO_3 was explored under normoxic (20% O_2) and hypoxic (1% O_2) conditions. HepG2 cells were prepared in glass-bottom culture dishes for 24 h. HepG2 cells were incubated with 0−10 μM Na_2SeO_3 for 12 h or 5 μM Na_2SeO_3 for 0−12 h and then incubated with 0.1 mg/mL nanoprobe in normoxic (20% O_2) and hypoxic (1% O_2) environments, respectively.[32] Before each step, the cells were washed three times with PBS. Fluorescence imaging was performed by using a confocal microscope with two channels. The green channel captured images using a 488 nm excitation, and the red channel captured images using a 633 nm excitation.

RESULTS AND DISCUSSION

Preparation and Characterization of the Mito-N-D-MSN. Mito-N-D-MSN was prepared by loading two fluorescent probes, DHE and NIR-H_2Se, in MSNs, subsequently attaching polyethylenimine to cap the pores of MSN, and modifying with triphenylphosphonium (TPP) ion to target mitochondria. The morphologies of the MSNs and Mito-N-D-MSN were characterized by TEM. The diameter of Mito-N-D-MSN was approximately 40 nm, and the morphology of the nanoprobe was not obviously different from that of the unmodified MSNs (Figure 1). The amounts of NIR-H_2Se and

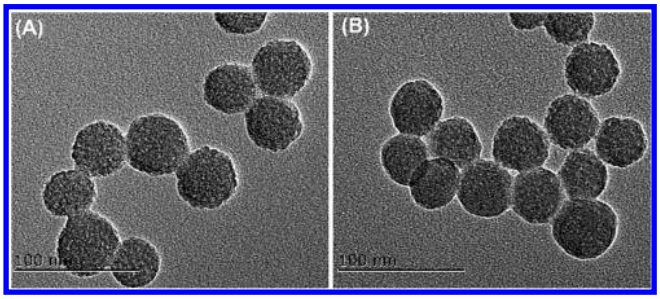

Figure 1. TEM image of MSNs (A) and Mito-N-D-MSN (B). Scale bars are 100 nm.

DHE loaded in the MSNs were calculated to be 7.0 mg/g and 6.0 mg/g, respectively (Figure S2). In addition, a zeta potential experiment was employed to confirm every step of the assembly of Mito-N-D-MSN (Figure S3), and the results confirmed that the nanoprobe was successfully assembled.

Response of Mito-N-D-MSN toward H_2Se and $O_2^{\bullet-}$. After preparation, the nanosphere was used as a fluorescent probe for H_2Se and $O_2^{\bullet-}$ detection. As shown in Figure 2A, an obvious fluorescence signal at 735 nm was observed in the absence of H_2Se, while significant fluorescence enhancements were observed with an increasing H_2Se concentration. There was a linear relationship between the fluorescence enhancement and H_2Se concentration in the range from 0 to 50 μM (Figure 2B). Figure 2C shows the changes in the fluorescence spectra of Mito-N-D-MSN in response to different concentrations of $O_2^{\bullet-}$. The addition of increasing concentrations of $O_2^{\bullet-}$ to Mito-N-D-MSN elicited a dramatic enhancement of the emission intensity at 638 nm, and there was good linearity of the relationship between the fluorescence intensity and $O_2^{\bullet-}$ concentration in the range of 0 to 50 μM (Figure 2D). The above results showed that Mito-N-D-MSN was able to individually or simultaneously monitor H_2Se and $O_2^{\bullet-}$ fluctuations without mutual interferences.

The effect of pH on the response of Mito-N-D-MSN to H_2Se and $O_2^{\bullet-}$ was studied. As shown in Figure S4, free Mito-

DOI: 10.1021/acs.analchem.8b01345
Anal. Chem. 2018, 90, 8116−8122

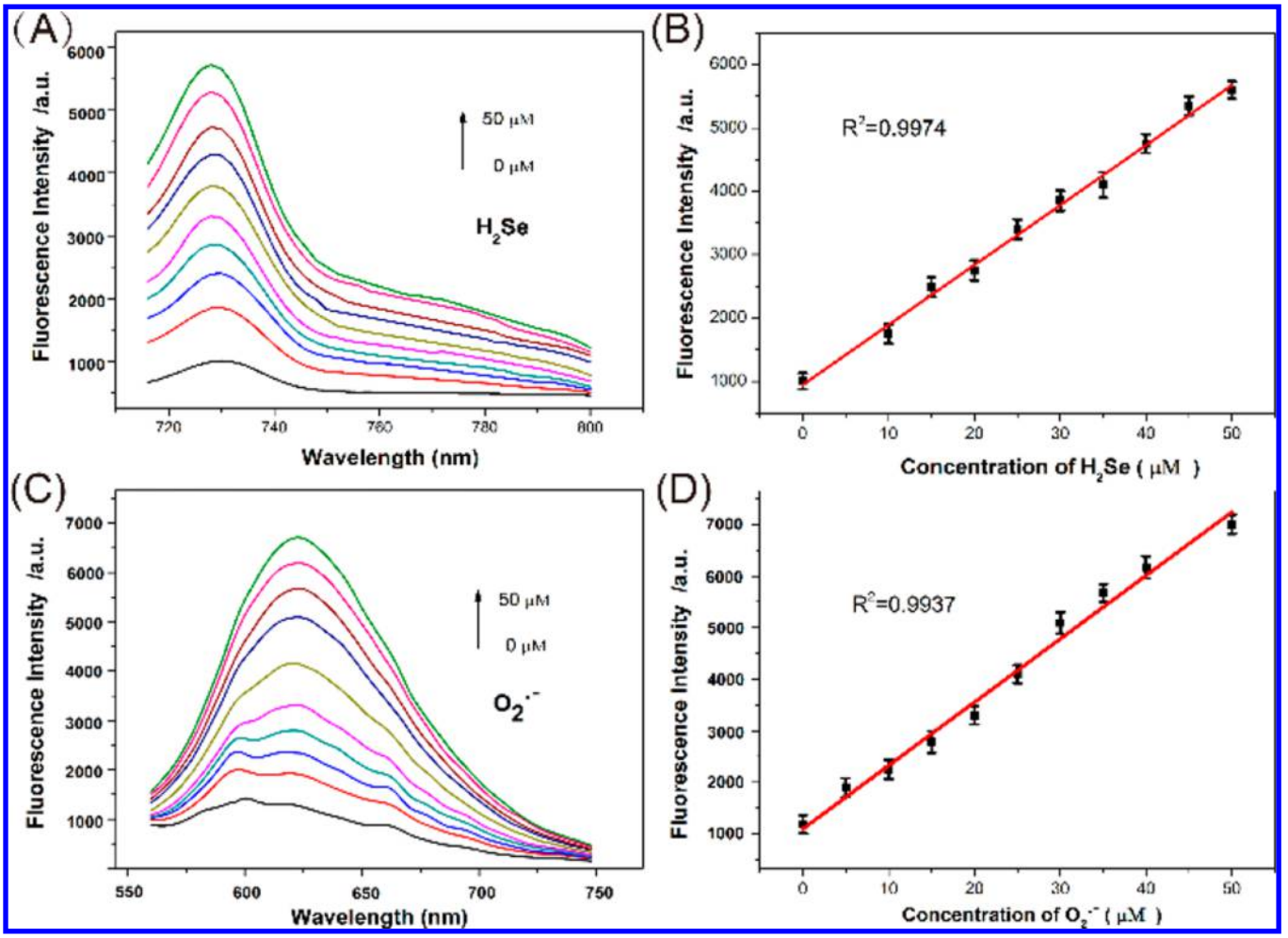

Figure 2. Fluorescence response of Mito-N-D-MSN to various concentrations of H_2Se and $O_2^{\bullet-}$ at room temperature in 10 mM PBS (pH = 7.8). (A) Fluorescence emission spectra of Mito-N-D-MSN with various H_2Se (λ_{ex} = 688 nm). (B) The linear correlation between the fluorescence intensity and the concentrations of H_2Se. (C) Fluorescence emission spectra of Mito-N-D-MSN with various $O_2^{\bullet-}$ (λ_{ex} = 488 nm). (D) The linear correlation between the fluorescence intensity and the concentrations of $O_2^{\bullet-}$.

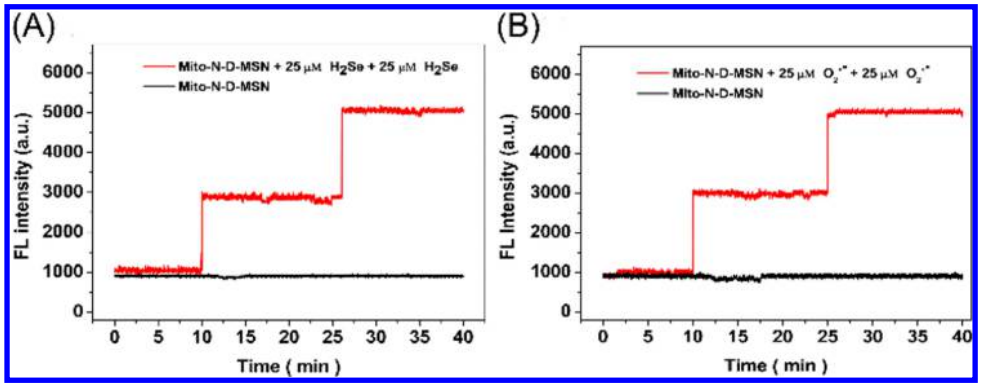

Figure 3. Kinetics experiments. (A) Time course of the fluorescence intensity of Mito-N-D-MSN during incubation with 25 μM H_2Se for 15 min, followed by the addition of another 25 μM H_2Se for 15 min (red line), compared with no H_2Se (black line) in 10 mM PBS, pH 7.8, at room temperature. (B) Time course of the fluorescence intensity of Mito-N-D-MSN during incubation with 25 μM $O_2^{\bullet-}$ for 15 min first, followed by the addition of another 25 μM $O_2^{\bullet-}$ (red line) for 15 min, compared with no $O_2^{\bullet-}$ (black line) in 10 mM PBS, pH 7.8, at room temperature.

N-D-MSN exhibited no significant fluorescence enhancement at 735 or 638 nm over a broad pH range (4.0−9.0), indicating that the nanoprobe was stable under physiological conditions. At 688 nm excitation, the addition of H_2Se induced remarkable fluorescence enhancement at 735 nm in the pH range 4.0−9.0. At 488 nm excitation, the addition of $O_2^{\bullet-}$ induced significant fluorescence enhancement at 638 nm in the pH range 4.0−9.0. These results suggest that Mito-N-D-MSN can function properly in biological environments.

To investigate the selectivity of Mito-N-D-MSN for detecting $H_2Se/O_2^{\bullet-}$, the responses of the nanoprobe toward some important interfering substances, such as metal ions,

DOI: 10.1021/acs.analchem.8b01345
Anal. Chem. 2018, 90, 8116−8122

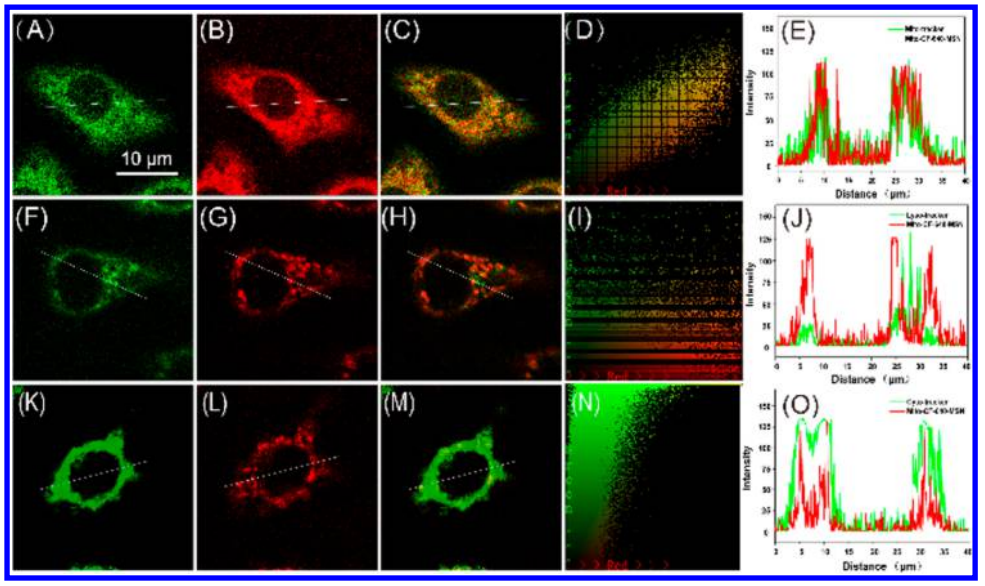

Figure 4. Mitochondria-targeting properties. Confocal fluorescence image of HepG2 cells treated with Mito-N-D-MSN. A, F, and K are the green channel for MTG, LTG, and CA respectively. B, G, and L are the red channel for Mito-N-D-MSN. C, H, and M are the overlay images of the green channel and the red channel. D, I, and N are the colocalization areas of the red and green channels selected. E, J, and O are the fluorescence intensity profiles of regions of interest across the white lines. Green channels are excited at 488 nm, while red channels are excited at 633 nm.

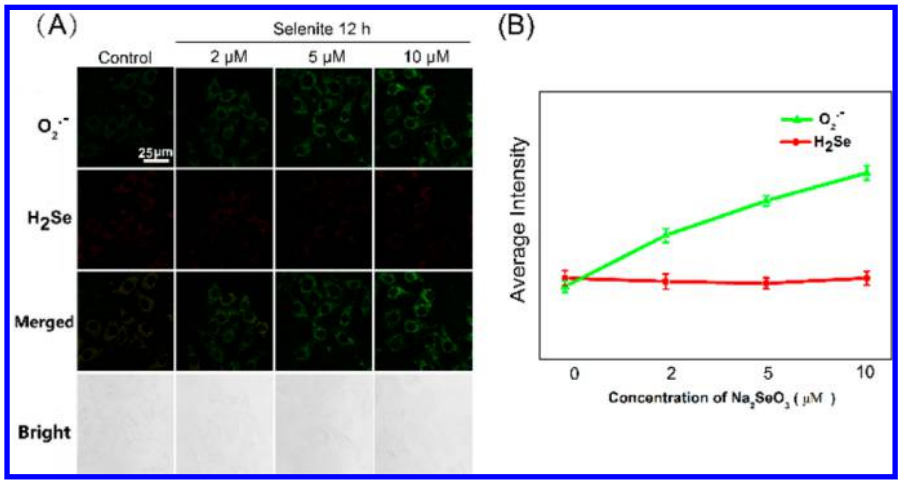

Figure 5. Confocal fluorescence images of H_2Se and $O_2^{\bullet-}$ in mitochondria of HepG2 cells treated with various concentrations of Na_2SeO_3 under normoxia (20% O_2) conditions. (A) Fluorescence changes in mitochondria for HepG2 cells exposed to different Na_2SeO_3 concentrations (2−10 μM) for 12 h and incubated with Mito-N-D-MSN (0.1 mg/mL). (B) Average fluorescence intensity. The fluorescence was imaged using a confocal microscope with 633 nm excitation which collection is 650−750 and 488 nm excitation which collection is 550−650 nm. Scale bar = 25 μm.

thiols (Cys, GSH, H_2S), vitamin C (Vc), selenium compounds ($(CysSe)_2$, Na_2SeO_3), a selenoprotein (TrxR), and biologically relevant ROSs, were tested. As shown in Figures S5, S6, and S7, there were no significant fluorescence changes in the presence of these interfering substances compared with the case of no added interfering substances, which demonstrated that Mito-N-D-MSN could recognize H_2Se and $O_2^{\bullet-}$ selectively under physiological conditions. In addition, the kinetics experiment revealed that the response of Mito-N-D-MSN to $H_2Se/O_2^{\bullet-}$ occurs instantly in pH 7.8 buffer, which enables the real-time detection of $H_2Se/O_2^{\bullet-}$ (Figure 3).

Colocalization Fluorescence Imaging. The MTT assay was used to detect different concentrations of Mito-N-D-MSN (0, 0.1, 0.2, and 0.3 mg/mL) for 6, 12, and 24 h, respectively. The nanoprobe concentration was 0.1 mg/mL, and the best incubation time was 12 h, as shown in Figure S8; we used these conditions to further explore the cell experiment. Calcein (CA), LysoTracker Green (LTG), and MitoTracker Green (MTG), which are commercially available targeting dyes for the cytoplasm, lysosomes and mitochondria, respectively, were used in colocalization experiments. The three commercial dyes were coincubated with Mito-CF-640-MSN HepG2 cells to label the relevant organelles before the imaging experiment. As shown in Figure 4, the green channel detects the commercial dye at 550−650 nm, and the red channel detects the nanoprobe at 650−750 nm. A well overlapped image of Mito-N-D-MSN and MTG (Pearson's correlation coefficient, ρ = 0.85) was evidenced by the clear yellow signals. By comparison, there was poor overlap between Mito-N-D-MSN and CA (ρ = 0.45) and poor overlap between the nanoprobe and LTG (ρ = 0.34). Obviously, Mito-N-D-MSN does not overlap with other organelles, such as the cytoplasm and lysosomes. The mitochondrial localization of the nanoprobe was also confirmed by SEM (Figure S9). These results

DOI: 10.1021/acs.analchem.8b01345
Anal. Chem. 2018, 90, 8116−8122

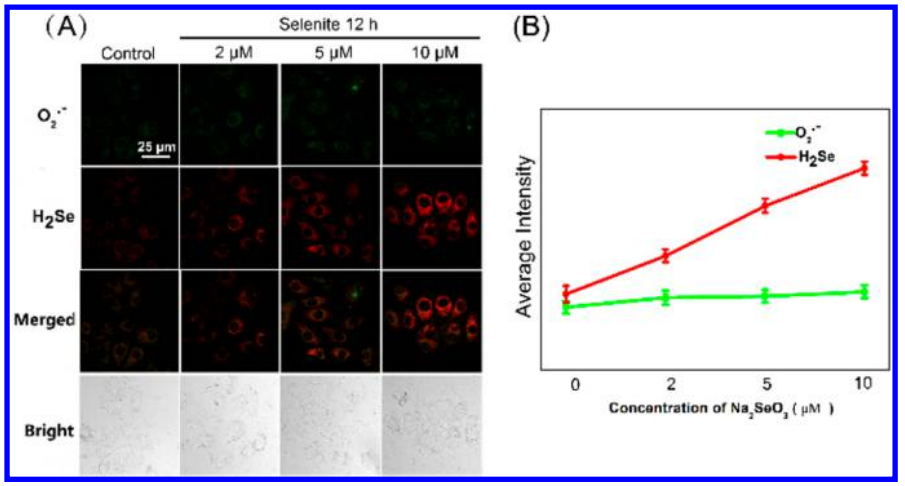

Figure 6. Confocal fluorescence images of H_2Se and $O_2^{\bullet-}$ in mitochondria of HepG2 cells treated with various concentrations of Na_2SeO_3 under hypoxia (1% O_2) conditions. (A) Fluorescence changes in mitochondria for HepG2 cells exposed to different Na_2SeO_3 concentrations (2−10 μM) for 12 h and incubated with Mito-N-D-MSN (0.1 mg/mL). (B) Fluorescence intensity for (A). The fluorescence was imaged using a confocal microscope with 633 nm excitation, which collection is 650−750, and 488 nm excitation, which collection is 550−650 nm. Scale bar = 25 μm.

proved that Mito-N-D-MSN could effectively target mitochondria.

Detection of Mitochondrial H_2Se and $O_2^{\bullet-}$ in HepG2 Cells under Normoxia and Hypoxia Condition. First, changes in the mitochondrial concentrations of H_2Se and $O_2^{\bullet-}$ in HepG2 cells induced by Na_2SeO_3 under normoxic (20% O_2) conditions were detected simultaneously. HepG2 cells were treated with 2−10 μM Na_2SeO_3 for 12 h under normoxia (20% O_2). As shown in Figure 5, higher $O_2^{\bullet-}$ contents were observed in mitochondria, while the H_2Se contents were low and remained unchanged under normoxic conditions. The fluorescence changes of HepG2 cells exposed to 5 μM Na_2SeO_3 for different durations (0−12 h) under normoxia (20% O_2) were also recorded, and similar results were obtained (Figure S10). These results showed that the Na_2SeO_3 anticancer mechanism consists of ROS-induced apoptosis in mitochondria under normoxic conditions.

Considering the hypoxic characteristic of solid tumors, we conclude that the mitochondrial redox status changes would be different in normoxic and hypoxic environments. To confirm this hypothesis, the changes in the mitochondrial H_2Se and $O_2^{\bullet-}$ contents in HepG2 cells induced by Na_2SeO_3 were detected simultaneously using Mito-N-D-MSN. HepG2 cells were treated with 2−10 μM Na_2SeO_3 for 12 h under hypoxia (1% O_2), and H_2Se and $O_2^{\bullet-}$ were simultaneously monitored using confocal imaging. The experimental results are shown in Figure 6. The H_2Se content increased obviously in the hypoxic environment, while the $O_2^{\bullet-}$ content level remained low in the hypoxic environment. HepG2 cells were exposed to 5 μM Na_2SeO_3 for different durations (0−12 h) and then incubated with the nanoprobe (0.1 mg/mL); similar results were obtained (Figure S11). The above results indicated that, in hypoxic environments, HepG2 cells induced by Na_2SeO_3 are exposed to a reducing environment, and the anticancer mechanism of selenite occurs via nonoxidative stress.

CONCLUSIONS

In summary, to elucidate the anticancer mechanism of selenite, we developed a nanoprobe, Mito-N-D-MSN, that can monitor mitochondrial H_2Se and $O_2^{\bullet-}$ changes simultaneously in living HepG2 cells. Mito-N-D-MSN can detect H_2Se and $O_2^{\bullet-}$ with high selectivity and sensitivity and was successfully applied to image H_2Se and $O_2^{\bullet-}$ simultaneously in HepG2 cells induced by Na_2SeO_3. The confocal fluorescence imaging results showed that under hypoxic conditions, the mitochondrial H_2Se content increased gradually while the $O_2^{\bullet-}$ content remained almost unchanged in HepG2 cells induced by Na_2SeO_3. The results indicated that the anticancer mechanism of selenite consists of nonoxidative stress in the real tumor microenvironment. We expect that this work will not only contribute to Na_2SeO_3-related studies but also provide a promising tool for further exploration of the anticancer mechanism of selenium-containing compounds.

ASSOCIATED CONTENT

Supporting Information

The Supporting Information is available free of charge on the ACS Publications website at DOI: 10.1021/acs.analchem.8b01345.

Supporting Figures S1−S11 (PDF).

AUTHOR INFORMATION

Corresponding Authors

*E-mail: xukehua@sdnu.edu.cn.
*E-mail: tangb@sdnu.edu.cn.

ORCID

Bo Tang: 0000-0002-8712-7025

Author Contributions

‡These authors contributed equally. The manuscript was written through contributions of all authors. All authors have given approval to the final version of the manuscript.

Notes

The authors declare no competing financial interest.

ACKNOWLEDGMENTS

This work was supported by the National Natural Science Foundation of China (21535004, 91753111, 21390411, 21575081, 21775091, 21507075).

REFERENCES

(1) Thomson, C. D. *Eur. J. Clin. Nutr.* **2004**, *58*, 391−402.

DOI: 10.1021/acs.analchem.8b01345
Anal. Chem. 2018, 90, 8116−8122

(2) Schrauzer, G. N. *Cell. Mol. Life Sci.* **2000**, *57*, 1864−1874.
(3) Clark, L. C.; Combs, G. F.; Turnbull, B. W.; Slate, E. H.; Chalker, D. K.; Chow, J.; Davis, L. S.; Glover, R. A.; Graham, G. F.; Gross, E. G.; Krongrad, A.; Lesher, J. L.; Park, H. K.; Sanders, B. B.; Smith, C. L.; Taylor, J. R. *JAMA* **1996**, *276*, 1957−1963.
(4) Rebsch, C. M.; Penna, F. J., 3rd; Copeland, P. R. *Cell Res.* **2006**, *16*, 940−948.
(5) Rayman, M. P. *Lancet* **2012**, *379*, 1256−1268.
(6) Wang, Y.; Fang, W.; Huang, Y.; Hu, F.; Ying, Q.; Yang, W.; Xiong, B. *Free Radical Biol. Med.* **2015**, *79*, 186−196.
(7) Björnstedt, M.; Kumar, S.; Holmgren, A. *J. Biol. Chem.* **1992**, *267*, 8030−8034.
(8) Wallenberg, M.; Olm, E.; Hebert, C.; Björnstedt, M.; Fernandes, A. P. *Biochem. J.* **2010**, *429*, 85−93.
(9) Shen, H. M.; Yang, C. F.; Ong, C. N. *Int. J. Cancer* **1999**, *81*, 820−828.
(10) Zhao, R.; Xiang, N.; Domann, F. E.; Zhong, W. *Cancer Res.* **2006**, *66*, 2296−2304.
(11) Yin, J.; Hu, Y.; Yoon, J. *Chem. Soc. Rev.* **2015**, *44*, 4619−4644.
(12) Ashton, T. D.; Jolliffe, K. A.; Pfeffer, F. M. *Chem. Soc. Rev.* **2015**, *44*, 4547−4595.
(13) Zhu, H.; Fan, J.; Wang, B.; Peng, X. *Chem. Soc. Rev.* **2015**, *44*, 4337−4366.
(14) Niu, J.; Fan, J.; Wang, Xu.; Xiao, Y.; Xie, X.; Jiao, X.; Sun, C.; Tang, B. *Anal. Chem.* **2017**, *89*, 7210−7215.
(15) Li, P.; Zhang, W.; Li, K.; Liu, X.; Xiao, H.; Zhang, W.; Tang, B. *Anal. Chem.* **2013**, *85*, 9877−9881.
(16) Kong, F.; Zhao, Y.; Liang, Z.; Liu, X.; Pan, X.; Luan, D.; Xu, K.; Tang, B. *Anal. Chem.* **2017**, *89*, 688−693.
(17) Zhang, Z.; Balogh, D.; Wang, F.; Willner, I. *J. Am. Chem. Soc.* **2013**, *135*, 1934−1940.
(18) Li, N.; Yu, Z. Z.; Pan, W.; Han, Y.; Zhang, T.; Tang, B. *Adv. Funct. Mater.* **2013**, *23*, 2255−2262.
(19) Li, Z.; Barnes, J. C.; Bosoy, A.; Stoddart, J. F.; Zink, J. I. *Chem. Soc. Rev.* **2012**, *41*, 2590−2605.
(20) Monaghan, R. M.; Barnes, R. G.; Fisher, K.; Andreou; Rooney, N.; Poulin, G. B.; Whitmarsh, A. J. *Nat. Cell Biol.* **2015**, *17*, 782−792.
(21) Yu, Z. Z.; Sun, Q. Q.; Pan, W.; Li, N.; Tang, B. *ACS Nano* **2015**, *9*, 11064−11074.
(22) Kong, F.; Ge, L.; Pan, X.; Xu, K.; Liu, X.; Tang, B. *Chem. Sci.* **2016**, *7*, 1051−1056.
(23) Matylitsky, V. V.; Shavel, A.; Gaponik, N.; Eychmüller, A.; Wachtveitl, J. *J. Phys. Chem. C* **2008**, *112*, 2703−2710.
(24) Kobler, J.; Möller, K.; Bein, T. *ACS Nano* **2008**, *2*, 791−799.
(25) Zhang, K.; Xu, L. L.; Jiang, J. G.; Calin, N.; Lam, K. F.; Zhang, S. J.; Wu, H. H.; Wu, G. D.; Albela, B.; Bonneviot, L.; Wu, P. *J. Am. Chem. Soc.* **2013**, *135*, 2427−2430.
(26) Yang, L. M.; Li, N.; Pan, W.; Yu, Z. Z.; Tang, B. *Anal. Chem.* **2015**, *87*, 3678−3684.
(27) Cao, L.; Zhao, Z.; Zhang, T.; Guo, X.; Wang, S.; Li, S.; Li, Y.; Yang, G. *Chem. Commun.* **2015**, *51*, 17324−17327.
(28) Wu, M. Y.; Li, K.; Liu, Y. H.; Yu, K. K.; Xie, Y. M.; Zhou, X. D.; Yu, X. Q. *Biomaterials* **2015**, *53*, 669−678.
(29) Si, F.; Liu, Y.; Yan, K. L.; Zhong, W. W. *Chem. Commun.* **2015**, *51*, 7931−7934.
(30) Kojima, H.; Nakatsubo, N.; Kikuchi, K.; Kawahara, S.; Kirino, Y.; Nagoshi, H.; Hirata, Y.; Nagano, T. *Anal. Chem.* **1998**, *70*, 2446−2453.
(31) Hung, M. C.; Mills, G. B.; Yu, D. *Nat. Med.* **2009**, *15*, 246−247.
(32) Kong, F.; Hu, B.; Gao, Y.; Xu, K.; Pan, X.; Huang, F.; Zheng, Q.; Chen, H.; Tang, B. *Chem. Commun.* **2015**, *51*, 3102−3105.

DOI: 10.1021/acs.analchem.8b01345
Anal. Chem. 2018, 90, 8116−8122